J. Phys. B: At. Mol. Opt. Phys. 27 (1994) 5773–5794. Printed in the UK

Covariance mapping mass spectroscopy using a pulsed electron ionizing source: application to CF_4

M R Bruce, L Mi, C R Sporleder and R A Bonham
Department of Chemistry, Indiana University, Bloomington, IN 47405, USA

Received 8 September 1994, in final form 17 October 1994

Abstract. We report the implementation of covariance mapping mass spectroscopy to pulsed-electron-beam ionization time-of-flight mass spectroscopy. The technique has been applied to CF_4 and evidence is presented for the previously unreported doubly coincident ionization channels: $CF_2^+ + F_2^+$, $CF^+ + F_2^+$, $CF_2^+ + F^+$, $F_2^+ + F^+$, $C^+ + F_2^+$, $F^{2+} + F^+$, $C^{2+} + F^+$, and $F^+ + F^+$ at electron impact energies of 100, 200, 300, 400 and 500 eV. In addition, indications for an unstable CF_4^+ parent ion are presented. Furthermore, sufficient statistics were accumulated to allow an attempt to determine the momentum distribution for the ions in several previously reported double ion channels ($CF_3^+ + F^+$, $CF_2^+ + F^+$, $CF^+ + F^+$, and $C^+ + F^+$) using a Monte Carlo method. Evidence for translational kinetic energies in excess of 10 eV was observed for some of the lighter ions. The magnitude of the resultant momentum from unobserved neutral fragments and the angle between the two detected ion momenta were calculated as well. The experiment was aided by the development of a fast data collection system. Contour maps of the major covariance mapping peaks were obtained with a time resolution of 16 ns at an experimental repetition rate of 50 kHz over a time-of-flight range of 8 μs.

1. Introduction

Observation of the production of two or more ions as the result of electron impact or photo absorption has been numerously reported (Besnard-Ramage *et al* 1989, Bruce *et al* 1992, Codling *et al* 1989, 1990, 1991, Creasey *et al* 1990, Curtis and Eland 1985, Eland 1987, Eland and Mathur 1991, Eland *et al* 1986a,b, Frasinski *et al* 1986, 1989a,b, 1991, Hagan and Eland 1991, Hatherly *et al* 1990, 1989, McCulloh *et al* 1965, Stankiewicz *et al* 1989, Ueda *et al* 1989, Winkoun and Dujardin 1986). The early experiments (Bruce *et al* 1992, Curtis and Eland 1985, McCulloh *et al* 1965) measured the difference in arrival times of the two ions in experiments dubbed PIPICO (photoion–photoion coincidence) (Curtis and Eland 1985). The occurrence of peaks in the difference spectrum signaled the presence of two ion break-up channels but with only a limited amount of additional information. In Eland *et al* (1986b) and Frasinski *et al* (1986) a new approach was reported in which the total flight time of each ion detected was recorded. The resulting data were plotted with the horizontal axis the flight time of the faster ion and the vertical axis the slower. The frequency of detected events was shown by frequency contours. This method, variously called covariance mapping spectroscopy (Frasinski *et al* 1986) or PEPIPICO (photoelectron–photoion–photoion coincidence) spectroscopy (Eland *et al* 1986b) represented a major advance over the PIPICO method since a great deal of additional information is obtained. In fact, a better terminology might be ion momentum spectroscopy. With the exception of McCulloh *et al* (1965) and Bruce *et al* (1992) these techniques have only been applied to photoionization using synchrotron light sources, UV line sources and multiphoton ionization using high power

0953-4075/94/235773+22$19.50

lasers. We wish to report here the first covariant mapping spectroscopy experiments using electron impact ionization. Our experiments have more in common with the synchrotron radiation experiments (e.g., Besnard-Ramage *et al* 1989, Eland *et al* 1986a) than the more recent multiphoton ionization work (e.g., Codling *et al* 1991, Frasinski *et al* 1991) in which an entire mass spectrum is obtained with a single laser pulse and covariance mapping is carried out by numerical computation for each single shot spectrum.

Covariance mapping mass spectroscopy has also been extended to the detection of three ions (Eland *et al* 1986b, Frasinski *et al* 1991). This type of spectroscopy can yield a great deal of useful information about the fragmentation of multi-charged ions as pointed out in the references cited and as described in the following. It would appear that it is also capable of providing cross section data of interest to radiation physics as well as to other applied areas such as the understanding of low pressure plasmas typically used in microelectronic fabrication. Furthermore, it is an ideal tool for detailed investigation of Coulomb explosion reactions in the threshold region.

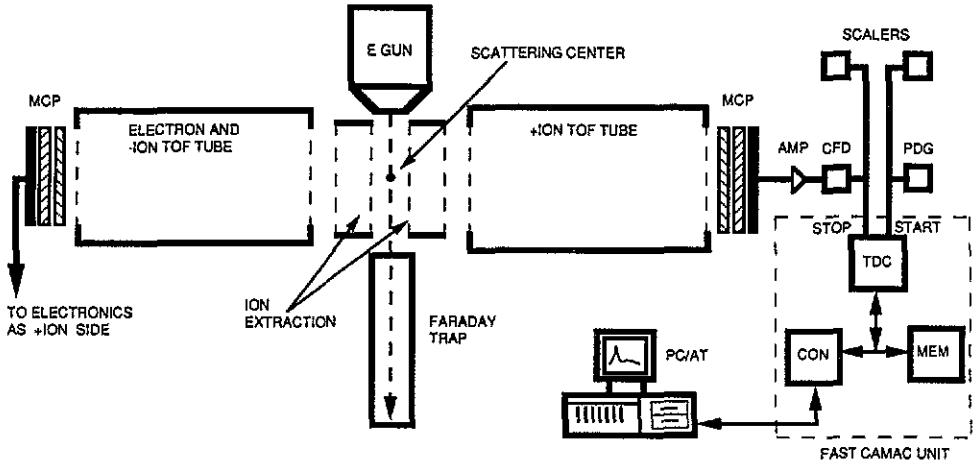

Figure 1. Schematic drawing of experimental apparatus. Acronyms: microchannel plate (MCP); time-of-flight (TOF); electron gun (E GUN); pre-amplifier (AMP); constant fraction discriminator (CFD); programmable delay gate (PDG); time-to-digital converter (TDC); fast CAMAC memory (MEM); fast CAMAC control module (CON).

2. Experiment

The apparatus employed for this experiment has been described elsewhere (Ma *et al* 1991, 1992). A schematic drawing of the main features is shown in figure 1. The electronics described in our earlier work (Ma *et al* 1991) were modified to attain an experimental repetition rate of 50 kHz with a time resolution of 16 ns over a time-of-flight (TOF) range of 8 μs. Small Computer Architecture Technology (SCAT) was employed with an Intel 286 based personal computer to collect the data. Typical covariant mapping spectra are shown in figures 2(*a*)–(*c*). These results can be compared to the photofragmentation spectrum obtained by Codling *et al* (1991). The data collection time in our case was about 100 hours and the incident electron energy was 100 eV in the case of figures 2(*a*) and 2(*b*) while figure 2(*c*) was obtained with 500 eV electrons; additional experiments were performed at

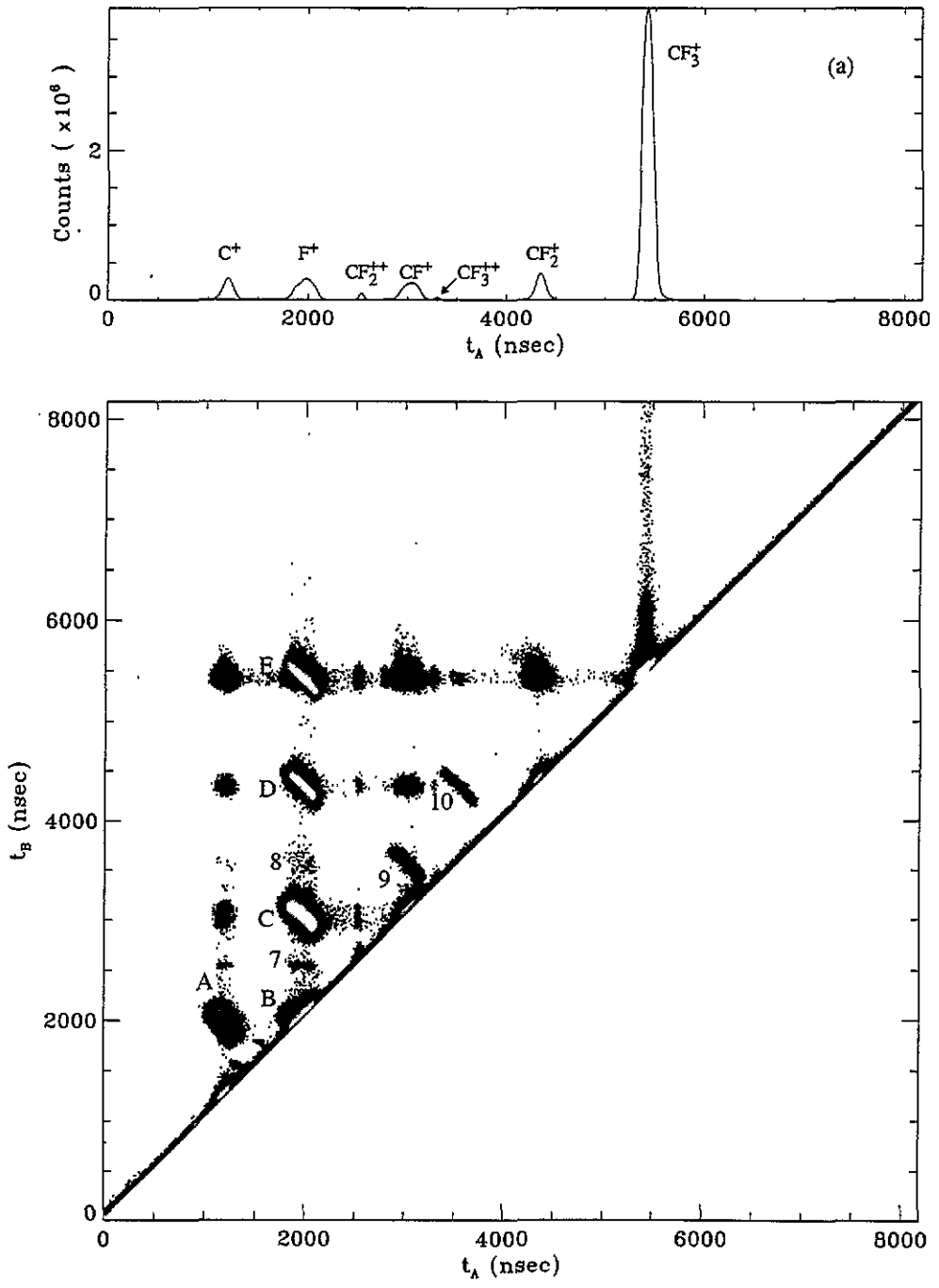

Figure 2. Covariant mapping/cross-correlation spectra of CF_4 taken at an electron impact energy of (*a*) 100 eV without accidental corrections (true data) (cross correlation spectra); (*b*) 100 eV with accidentals covariantly subtracted out (covariance mapping); (*c*) 500 eV with accidentals covariantly subtracted out (covariance mapping). The major features are assigned as: A, $C^+ + F^+$; B, $F^+ + F^+$; C, $F^+ + CF^+$; D, $F^+ + CF_2^+$; E, $F^+ + CF_3^+$; while the minor features are assigned: 1, $C^{2+} + F^+$; 2, $F^{2+} + C^+$; 3, $F^{2+} + F^+$; 4, $F^{2+} + CF^+$; 5, $C^+ + F_2^+$; 6, $CF^{2+} + F^+$; 7, $F^+ + CF_2^{2+}$; 8, $F^+ + F_2^+$; 9, $CF^+ + F_2^+$; 10, $F_2^+ + CF_2^+$. Unlabelled features are attributed to accidental (false) coincidences, or residues from accidental subtraction.

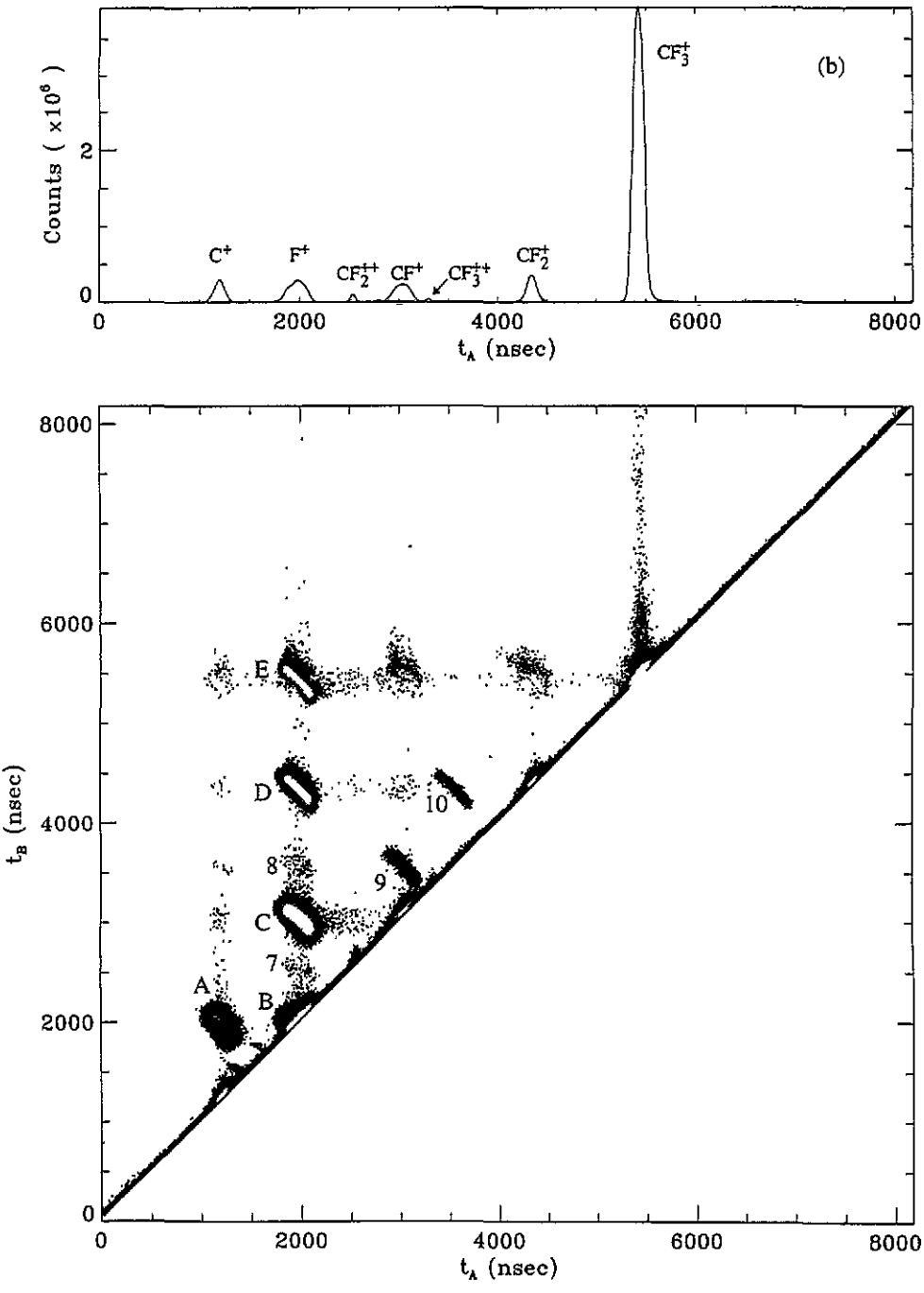

Figure 2. (Continued)

electron impact energies of 200, 300 and 400 eV. The spectrum displayed in figure 2(*a*) is an actual spectrum including accidental as well as coincident events. In figures 2(*b*) and 2(*c*) the accidental events have been subtracted out as explained later. The electron pulse width was 40 ns and a 150 V cm^{-1} extraction field with a 3 ns rise time was turned

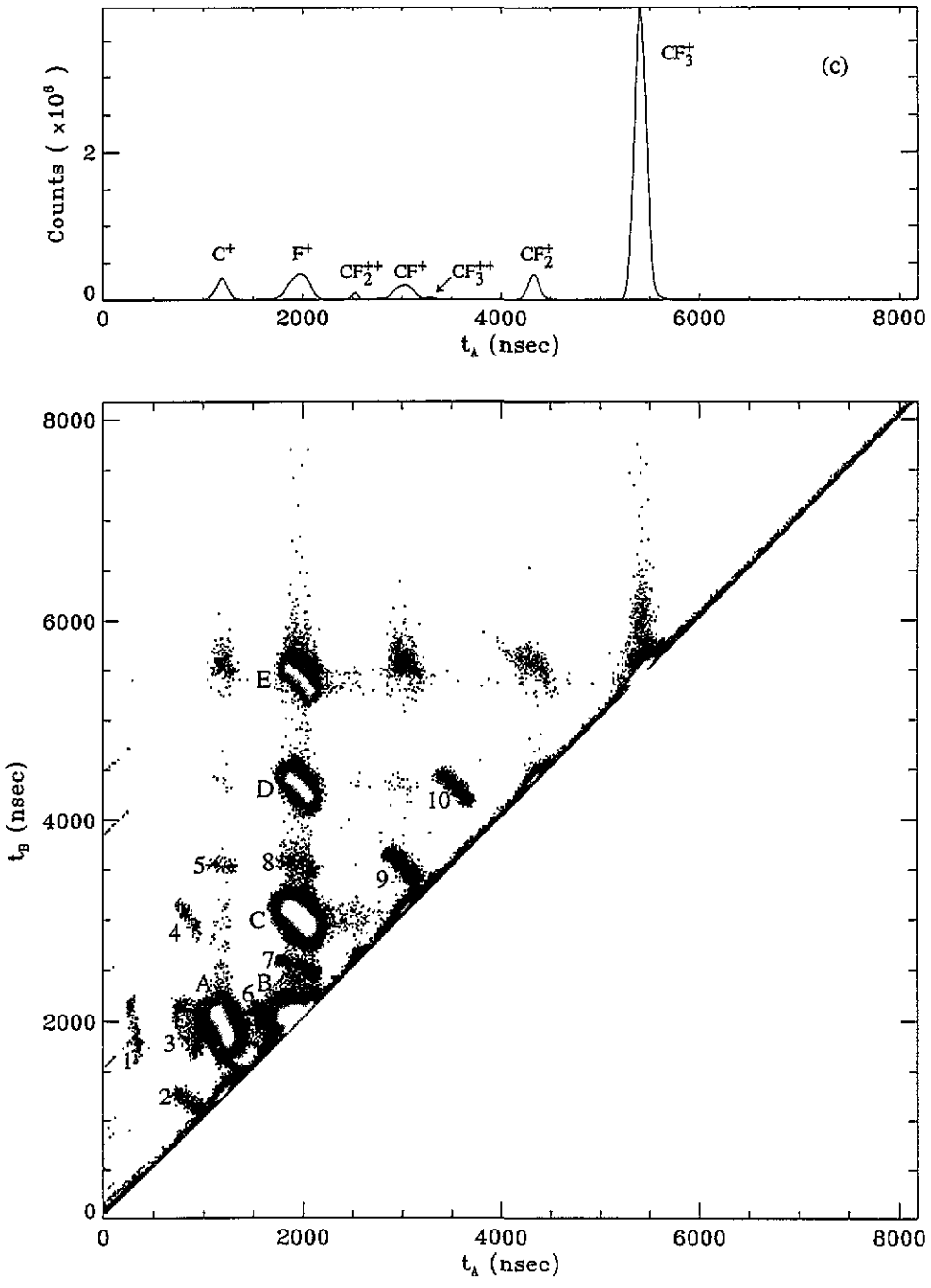

Figure 2. (Continued)

on 10 ns after the ionizing electron pulse cleared the ionization region. The extraction field consisted of 90 V applied to each of the two extraction grids but with opposite sign. The grids are spaced 12 mm apart and the ionization region lies half way between them. After reaching the negatively charged extraction grid the positive ions coasted in a constant

field for 25 mm and were then accelerated up to 600 V over a distance of 6 mm. They then drifted in a constant field for 150 mm and finally were accelerated through a potential difference of 2.75 kV over 6 mm, where they encountered the front face of a 40 mm diameter microchannel plate detector. All constant potential regions were separated by 90% optically transparent gold mesh grids. The extent to which all ions in our experiment are detected with the same efficiency has been explored elsewhere (Bruce and Bonham 1992).

The present design of our apparatus is not optimum for covariant mapping experiments with translationally hot ions (Codling *et al* 1991). A new apparatus, with 30 mm flight distance from ion source to detector, and with a 100% kinetic energy detection range (not counting grid and detector efficiency losses) of 0–40 eV, is currently under construction. The 100% collection efficiency range of the present instrument is only 0–6 eV. The subsequent mass resolution loss in the new instrument will be partially compensated by increasing the timing resolution to 1 ns and by using a redesigned electron gun with tighter focusing. It should be noted that a shorter flight distance should enhance our ability to observe metastable species (Van der Burgt and McConkey 1991).

In our experiments a cross correlation spectrum between first arrival ions and second arrival ions is recorded. A singles spectrum, consisting of all experiments in which only one ion is detected, is simultaneously recorded and used to calculate an autocorrelation function. This function, except for a scaling factor, is exactly the spectrum of accidental coincidences. As long as one or more isolated coincidence peaks in the cross correlation spectrum can be assigned uniquely as being accidental (i.e. events coming from different molecules—has zero covariance) it is possible to place the autocorrelation spectrum of accidentals on the same scale as the cross correlation spectrum and to subtract it out. The result is a covariance function which has been referred to as a covariance mapping mass spectrum (Codling *et al* 1990, Frasinski *et al* 1989b). Rigorously, the scaling factor should be the reciprocal of the total number of experiments run and hence scaling should not have to depend on the existance of isolated accidental peaks in the spectrum. In practice we have found that the scale factor based on matching to accidental peaks is nominally 10% lower than the reciprocal of the estimated number of experiments (the difference is attributed to loss of experiments during computer processing time). In the case of CF_4 there are six strong accidental peaks as can be seen in figure 2a (unlabelled features), identified as such since they contain correlations between two fragments both of which contain carbon atoms. They are primarily circular in shape in contrast to the true coincidences which are elongated ellipses whose major axes are roughly diagonal to the horizontal axis (a full explanation of the shapes is in the theory section). We have minimized the size of the accidental correction by collecting pairs of events with a count rate that is purposely made very small. This can be accomplished because the accidental occurrence of two ions, coming from different molecules, depends on the square of the target gas density while a true coincident event is directly proportional to the target gas density. The low coincidence rate due to the use of a weak effusive gas jet target to minimize accidental coincidences is partly compensated by use of a high experimental repetition rate (50 kHz). Note that if the ocurrence of accidentals could be completely surpressed that the cross correlation and the covariance matrix mass spectrum would be exactly the same. Finally, it should be noted, that of all the true features observed in figures 2(*a*)–(*c*), the only one with any substantial accidental contribution was $CF_3^+ + F^+$—accidentals accounted for typically 10–20% of the integrated peak intensity in the cross correlation spectrum (figure 2(*a*)).

In figures 3(*a*)–(*d*) we show the covariantly corrected contour maps at a timing resolution of 16 ns for the four main coincidence peaks corresponding to the break-up reactions with the final ion products: $CF_3^+ + F^+$, $CF_2^+ + F^+$, $CF^+ + F^+$, and $C^+ + F^+$; in particular,

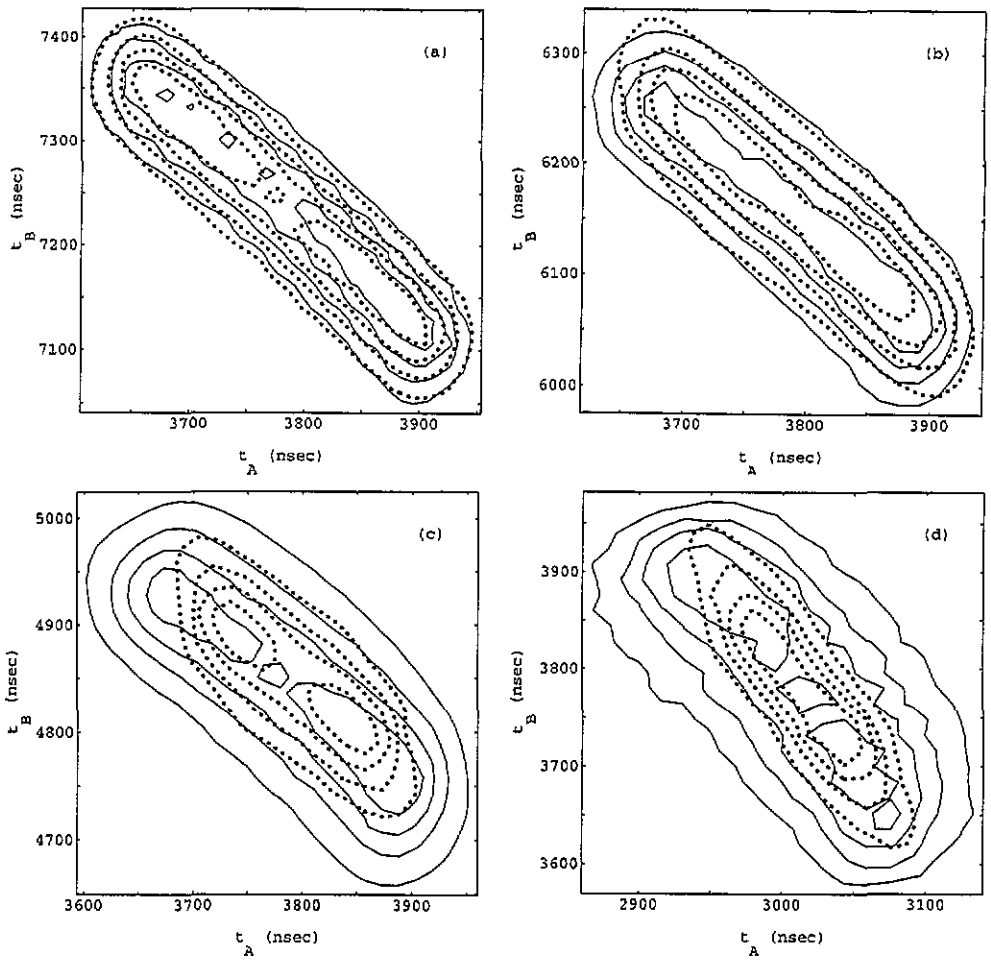

Figure 3. Contour maps for the dominant ion–ion coincidence features observed in figure 2(*b*) (false coincidences have been removed): (*a*) $CF_3^+ + F^+$; (*b*) $CF_2^+ + F^+$; (*c*) $CF^+ + F^+$; (*d*) $C^+ + F^+$. Experimental contours are represented by full lines while contours from a Monte Carlo simulation (see sections 3 and 4.3) are represented by dotted lines. Contour spacing is $\frac{1}{4}$ of maximum: (*a*) 1497, (*b*) 1446, (*c*) 1962, (*d*) 618.

the pure elliptical shape for $CF_3^+ + F^+$ attest to how well the correction procedure works when compared to the original shape seen in figure 2(*a*). Moreover, such detailed contour maps with 3% counting statistics near the maxima warrant the use of a more sophisticated theoretical interpretation than previously employed (Codling *et al* 1991).

3. Theory

3.1. Assumptions

Two approaches can be used to analyze the covariance mapping features, in addition to the purely statistical interpretation (Eland 1987), providing one is willing to make certain physical assumptions about the break-up process. The first approach involves explicit use of energy and momentum conservation. This approach has been extensively used by Eland

(1987) to discuss the dynamics of three body break-up reactions. This approach has the advantage that some information concerning sequential steps in the break-up can be obtained. Unfortunately the interpretation of the data, we believe, is not unique unless the lifetimes involved exceed the time resolution of the experiment. Hence, we will test a simpler model, which can be used for two body or more break-up reactions, previously referred to as an instantaneous explosion mechanism (Eland 1987). This approach involves, what we shall call, the implicit use of linear momentum conservation. Energy conservation is not explicitly assumed in this model. Our immediate goal is to take a simple model and force it to give the best fit possible to our data. A good fit will not prove the assumed mechanism to be correct nor will it prove it to be wrong. However, a poor fit will definitely rule it out. We believe that our data is the first to be obtained, for any molecule, with contour maps of major peaks with our statistical accuracy. Hence, we feel that a careful comparison with a simple model is justified. For the first time, an attempt will be made to obtain the detailed shape of ion momentum distributions from covariance matrix mass spectral peaks.

The assumptions of this model are as follows.

(i) The doubly (multiply) charged precursor ion to a break-up reaction is assumed to have zero linear momentum or a momentum that is negligible in comparison to break-up ion momenta.

(ii) Each of the two observed ions in a break-up reaction has a well defined linear momentum. A particular choice for the value of one momentum is always paired with a unique value of the other or at least a narrowly peaked distribution of allowed values for the second ion's momentum. The angle between the two momenta is also assumed fixed or at least distributed in a narrow peak for each break-up reaction.

(iii) The sum of all unobserved momenta in any break-up reaction can be replaced by a resultant momentum vector and the sum of this momentum vector with the other two ion momenta must add to zero (conservation of linear momentum).

(iv) The directions in space relative to a fixed laboratory coordinate frame for the momenta in all reactions with the same break-up momenta are randomly distributed (the target molecules are neither oriented nor aligned and the probe projectile is unpolarized).

As will be shown below these assumptions make it possible to extract values for the magnitudes of the two ion momenta and the angle between them from contours of the maps shown in figure 3. In addition, in the case of break-up reactions, with one or more unobserved fragments, it is possible to extract the magnitude of the vector sum for the unobserved momenta and the angles between it and the two ion momenta from each contour (e.g. from figures 3(*b*)–(*d*)). Failure of this model to explain the observed data would signify the existence of more complicated dynamics. In order to apply the model in the most rigorous fashion we will use Monte Carlo simulations to refine the agreement between experiment and model predictions. A simplified treatment using the model is first developed to obtain estimates of the parameters to be refined by the Monte Carlo procedure.

The total flight time, t_A, for an ion, designated as A, in our geometry is given by the expression

$$t_A = -\left(\frac{z_1}{E_1}\right) P_z^A + t_0^A(z_n, V_n, M_A, (P_z^A)^2) - \left(\frac{z_1}{E_1}\right) P_z^A + t_0^A(z_n, V_n, M_A, 0)\left[1 + \frac{(P_z^A)^2}{4M_A E_1} + \ldots\right] \quad (1)$$

where z_1 is the distance in the draw out direction from the ion formation point to the first grid, E_1 is the energy acquired by either ion during the extraction (i.e. the kinetic energy

at the first grid) assuming each ion has unit charge, P_z^A is the projection of the ions initial momentum on an axis parallel to the direction of the extracting electric field, the z_n represent distances to various grids (measured from the centre of the ionizing region), the V_n represent the potentials on these same grids, and M_A is the mass of the ion. We will use the letter A to label the first ion to be detected (fastest) and B to label the second ion to be detected (slowest). The important points to note are:

- the flight time differences, $t_{A,B} - t_0^{A,B}(z_n, V_n, M_A, 0)$, can be expanded in a power series in the initial momentum in which all terms depend on even powers of the momentum with the exception of the first-order term in the expansion which is linear in the initial momentum;
- the total flight time has a very weak dependence on the ion's initial kinetic energy in the draw out direction (i.e. the even powers of the initial momentum in the expansion in equation (1)).

The latter follows from the fact that the ions initial kinetic energy is generally less than 10 eV while the energy attained in the extraction field is 90 eV. Hence the lowest-order correction will generally be less than 5%. In this work we will ignore the corrections of the order of $(P_z^A)^2/(4M_AE_1)$ and higher in the expression for the total flight time, since calculations using our experimental parameters have shown such corrections to be negligible. Also note that $t_0^A(z_n, V_n, M_A, 0)$ is the ion flight time for break-up reactions where the initial momentum of ion A is perpendicular to the extraction direction (i.e. $P_z^A = 0$). The weak dependence of the total flight time on the initial kinetic energy of the ion in the draw out direction has been previously noted (Eland *et al* 1986b, Frasinski *et al* 1986) and becomes even weaker as the flight tube is shortened.

3.2. Analysis

In what follows, it will be convenient to define the apparatus dependent experimental quantity γ as

$$\gamma = \left(\frac{z_1}{E_1}\right) \tag{2}$$

where it should be noted that in the cases where an ion has more than one unit of electronic charge E_1 will have to be replaced by $q_{A,B}E_1$ where $q_{A,B}$ is the number of electronic charges on the ion. For this reason we will introduce the ion charge number $q_{A,B}$ to avoid making γ ion charge dependent.

With the assumptions in section 3.1, the parametric equations for a contour for the two coincident ions with a particular choice of the values of momenta can be written as

$$t_A \simeq -\left(\frac{\gamma}{q_A}\right) P_z^A + t_0^A(z_n, V_n, M_A, 0) \tag{3}$$

$$t_B \simeq -\left(\frac{\gamma}{q_B}\right) P_z^B + t_0^B(z_n, V_n, M_B, 0). \tag{4}$$

For the case where the two ion momenta directions are not collinear we can take P_z^A as a unique projection of the momentum P_A but then P_B will not be uniquely defined since for a fixed orientation of P_A all orientations of P_B about P_A for a fixed value of the angle between them, θ_{AB}, are equally probable. The probability for finding the value P_z^B for the

projection of the vector P_B on the draw out direction is given by the vector model as (see Brink and Satchler 1968, equation (2.26))

$$\rho\left(P_z^B\right) = \left(\frac{1}{\pi}\right)\left\{P_B^2 \sin^2\alpha - \left[(P_z^B)^2 + (P_B\cos\theta_{AB})^2 - 2P_z^B P_B \cos\theta_{AB}\cos\alpha\right]\right\}^{-1/2}. \quad (5)$$

This distribution function is strongly peaked at the two values

$$P_z^{B(\pm)} = P_B\cos(\theta_{AB} \pm \alpha)$$

where α is the angle between the draw out direction and the vector P_A. This suggests approximating the probability by two Dirac delta functions

$$\rho\left(P_z^B\right) = \delta\left[P_z^{B(+)} - P_B\cos(\theta_{AB}+\alpha)\right] + \delta\left[P_z^{B(-)} - P_B\cos(\theta_{AB}-\alpha)\right]. \quad (6)$$

By use of equation (6) and the substitution $P_z^A = P_A\cos\alpha$, the parametric equations (3) and (4) can be written as

$$\frac{(t'_A)^2}{(a)^2} + \frac{(t'_B)^2}{(b)^2} = 1 \quad (7)$$

where

$$a = \frac{\gamma P_A P_B \sin\theta_{AB}}{[(q_B P_A \sin\phi)^2 + (q_A P_B\cos\phi)^2 - q_A q_B P_A P_B \sin(2\phi)\cos\theta_{AB}]^{1/2}} \quad (8)$$

$$b = \frac{\gamma P_A P_B \sin\theta_{AB}}{[(q_B P_A \cos\phi)^2 + (q_A P_B\sin\phi)^2 + q_A q_B P_A P_B \sin(2\phi)\cos\theta_{AB}]^{1/2}} \quad (9)$$

$$\phi = \tfrac{1}{2}\arctan\left(\frac{2q_A q_B P_A P_B\cos\theta_{AB}}{(q_B P_A)^2 - (q_A P_B)^2}\right) \quad (10)$$

and the relationship between the old and new coordinate system is given by the transformation

$$\begin{bmatrix} t'_A \\ t'_B \end{bmatrix} = \begin{bmatrix} \cos\phi & \sin\phi \\ -\sin\phi & \cos\phi \end{bmatrix}\begin{bmatrix} t_A - t_0^A(z_n, V_n, M_A, 0) \\ t_B - t_0^B(z_n, V_n, M_B, 0) \end{bmatrix}. \quad (11)$$

Equation (7) can be readily recognized as the parabolic equation for an ellipse whose major axis makes an angle ϕ with the horizontal time axis (t_A); this defines the general shape of a single contour for two coincident ions with a particular choice of values for the momenta. If the full equation (5) is used, the elliptical contour will be filled in, and thus the analysis predicts that the shape of a three dimensional plot of the frequency of observed events plotted as a function of t_A on the horizontal axis and t_B on the vertical axis will yield approximately elliptically shaped peaks for true coincidence events. For the case of accidental events, the angle θ_{AB} and the relationship of the momenta for ions A and B is uncorrelated (not unique) and therefore the peaks will be approximately circularly shaped; this behaviour can be observed in figure 2(*a*).

A theoretical profile, based on equation (7), for a single contour is shown in figure 4. The critical points on the contour are shown for two coincident ions with a particular choice for the values of the momenta; the ellipse can be further characterized by the time difference parameters Δt_A, Δt_B, $\Delta t_\perp$, $\Delta t_\parallel$, and the angle ϕ that the principal axis of the ellipse makes

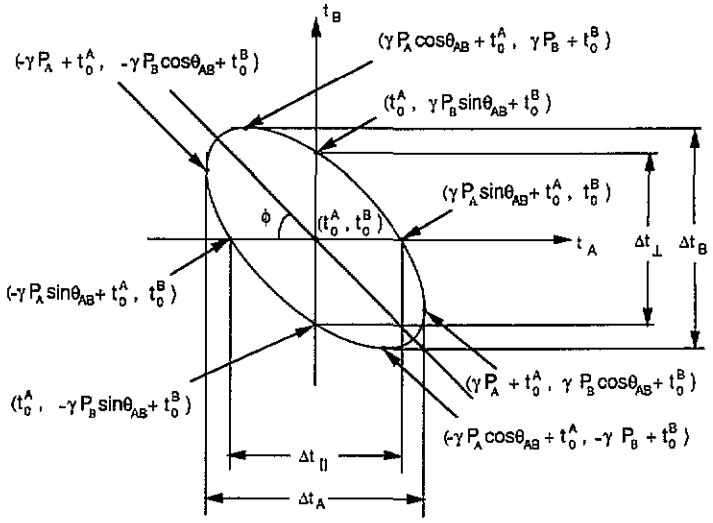

Figure 4. Theoretical single contour profile (ellipse) for a covariant mass spectra. $\Delta t_{A,B}$, maximal time deviation of profile on horizontal/vertical axis, respectively; $\Delta t_{\perp,\parallel}$, time difference on t_A and t_B axis, respectively, through centre (t_0^A, t_0^B) of ellipse; ϕ, angle that the principle axis of the ellipse makes with the t_A axis. See text in section 3 for further details.

with the t_A axis; these quantities are defined in figure 4. With these parameters introduced it is possible to write the magnitude of the two ion momenta, $P_{A,B}$, and the angle between them, θ_{AB}, as

$$P_{A,B} = q_{A,B}\left(\frac{\Delta t_{A,B}}{2\gamma}\right) \tag{12}$$

and

$$\theta_{AB} = \arcsin\left(\frac{\Delta t_\perp}{\Delta t_A}\right) = \arcsin\left(\frac{\Delta t_\parallel}{\Delta t_B}\right). \tag{13}$$

The angle, ϕ, that the major axis of each ellipse makes with the horizontal time axis is sensitive to the charges on the two coincident ions as can be seen from the approximate relationship

$$\phi \simeq \arctan\left(\frac{\Delta t_B}{\Delta t_A}\right) \simeq \arctan\left(\frac{q_A P_B}{q_B P_A}\right). \tag{14}$$

Equations (12) through (14) are generally useful for making estimates, and accordingly they will be used for the initial guesses to start off the Monte Carlo procedure discussed in the next section.

For the special case of a collinear break-up reaction momentum conservation requires that the shape of contours converges to one line and the tangent of the angle ϕ is just the ratio of the charge on ion A to the charge on ion B. In the case of three or more body break-up reactions both the angle ϕ and the length of the minor axis of the ellipse are highly correlated with the vector sum of the unobserved momenta. If the associated fragments have the same charge, an angle of 45° to the horizontal axis indicates that the

two charged particles have the same momentum. Any broadening (increase in the length of the minor axis) of the ellipse over that observed from the width of a known binary break-up peak (broadening of the binary peak is due to the finite widths of the electron beam and effusive gas jet target) can be used to calculate the decrease in the angle θ_{AB} from 180°. An angle ϕ greater than 45°, as seen in figure 3d, implies that the slower ion has a larger momentum than the faster ion (providing both have the same charge). In this case the ions have the same momentum distribution but with different momentum scales.

It is important to note that all the experimental contours of each break-up reaction in figure 3(*b*)–(*d*) have the same shape. This behaviour confirms our assumption of constant θ_{AB} and predicts that the values of momenta for the two coincident ions are proportional and hence the angle ϕ is constant for each break-up reaction; however, as a caution, this may not always be the case (Eland 1987). Since the angle ϕ is fixed for each break-up reaction, the most precise way we have discovered for determining the value of ϕ is to treat each contour as a two dimensional rotating object with t_A and t_B as x and y position coordinates and the frequency as a continuous mass (weighting) variable. Using these analogies a two-dimensional inertial tensor is constructed and ϕ is defined as the angle through which the laboratory time axes must be rotated in order to diagonalize the tensor (principal axis) (e.g. see Becker 1954 equation (12.16) with z=0).

3.3. Monte Carlo simulation

As pointed out in the experimental section, in cases where counting statistics make it feasible, the data can be plotted as a contour map of constant frequency with each data point representing the total number of events in a time box 16 ns on each side (see figures 3(*a*)–(*d*)). Such detailed contour maps warrant the use of a more sophisticated Monte Carlo method to simulate the experimental data.

Monte Carlo calculations were carried out by optimizing the parameters: θ_{AB}, a proportionality constant relating the magnitude of two coincident momenta given by

$$C_{AB} = \frac{P_A}{P_B} \tag{15}$$

and the momentum distribution for both coincident ions (assumes the same form for both distributions). The values for the parameters were initially chosen based on the simpler analysis made in the last section (i.e., equations (12)–(14)). FORTRAN and MATHEMATICA programs were written to simulate the experimental process. The calculation was performed by generating randomly distributed momentum pairs of the two coincident ions, then finding the corresponding time box for each event according to their flight time and calculating the total number of events in the time boxes. The best result was obtained by comparing a histogram constructed from the Monte Carlo result with the experimental data as can be seen in figures 3(*a*)–(*d*). The details of the calculation are described as follows.

The magnitude of P_A was randomly generated based on the *a priori* momentum distribution. Since all orientations of the vector P_A are equally probable, a uniformly distributed random number from 0 to π was generated representing the angle α that the vector P_A makes with the draw out direction. The total flight time, t_A, for the ion A is computed by equation (3) where the projection (P_z^A) of the vector P_A on the draw out direction is given by

$$P_z^A = P_A \cos\alpha \tag{16}$$

and z_1 via γ in equation (2) is randomly selected and weighted by the product distribution resulting from the gas jet and electron beam distributions. The product distribution was obtained by fitting the $CF_3^+ + F^+$ coincidence peak. Having generated the vector P_A, the magnitude of the momentum for ion B is determined by use of equation (15). The projection (P_z^B) of vector P_B on the draw out direction with constant angle θ_{AB} between the vectors P_A and P_B is

$$P_z^B = P_B(\cos\theta_{AB}\cos\alpha - \sin\theta_{AB}\sin\alpha\cos\varphi) \tag{17}$$

where φ is a uniformly distributed random number from 0 to 2π representing the azimuthal angle about the vector P_A; this results from the fact that all orientations of vector P_B about vector P_A with a fixed value of the angle θ_{AB} between them are equally probable. The total flight time, t_B, for the ion B is then computed from equation (4). Once t_A and t_B have been determined, the total number of events in the corresponding time box is increased by one. The process is repeated until the maximum total number of events in all the time boxes equals that of the experimental data. The resultant Monte Carlo data can be plotted as a contour map and compared with the experimental result, as shown in figures 3(*a*)–(*d*). After the comparison, corrections to the momentum distribution, C_{AB}, and θ_{AB} are made until the best possible agreement is achieved.

One caveat concerns the accuracy of equation (1) in the simulation. This equation is an approximate treatment of the ion trajectories and does not allow for the inclusion of transmission grid effects. Our presently available computer system for calculating ion trajectories in such electric fields possesses insufficient resolution and speed to model such effects. The first-order linear time-momentum was chosen from equation (1) to save computational time; fortunately, for our experimental situation the momentum distribution was found to only weakly depend on the higher-order terms in equation (1) when they were included.

An experimental artifact that was included in the simulation concerns the loss of highly energetic ions. In the actual experiment, if any one of the two coincident ions has a large initial velocity component (> 6 eV) perpendicular to the draw out direction, the faster ion will miss the detector and the coincident event will be lost. In the Monte Carlo simulation, the same restriction can be placed on the calculation; namely, if

$$\frac{P_{xy}^B t_B}{M_B} \text{ or } \frac{P_{xy}^A t_A}{M_A} \geqslant R_f \tag{18}$$

where

$$P_{xy}^{A,B} = [(P_{A,B})^2 - (P_z^{A,B})^2]^{1/2} \tag{19}$$

and R_f is the inner radius of the flight tube (20 mm), then the ion will hit the wall of the flight tube and, hence, these events will be eliminated in the Monte Carlo simulation as well. Further limitations of the theory are discussed in section 4.3 along with the results from the Monte Carlo calculation.

4. Results for CF_4

4.1. Cross sections (abundances)

In table 1 are listed the cross sections (abundances) determined from this study. The absolute numbers were determined by scaling the CF_3^+ intensity to the cross sections from Bruce and

Table 1. Absolute ion pair production cross sections (σ) for electron impact dissociative double ionization of CF_4. The numbers in parenthesis are cross sections from an earlier work (Bruce *et al* 1992). The units for the cross section σ are 10^{-20} m^2.

	σ				
Ion pair	100 eV	200 eV	300 eV	400 eV	500 eV
$F^+ + C^+$	4.1 (3.7)	14.4 (9.2)	14.1 (10.1)	11.5 (7.4)	10.4 (6.4)
$CF^+ + F^+$	14.2 (13.1)	26.1 (21.5)	23.4 (20.6)	19.6 (16.9)	17.6 (14.7)
$CF_2^+ + F^+$	7.6 (7.4)	9.9 (8.9)	8.6 (8.1)	7.3 (6.8)	6.5 (5.8)
$CF_3^+ + F^+$	7.1 (6.3)	8.3 (7.5)	7.2 (6.3)	6.0 (5.4)	5.5 (4.6)
$F^+ + F^+$	2.5	11.7	12.3	10.1	9.8
$CF_2^+ + F_2^+$	0.12	0.14	0.11	0.11	0.09
$CF^+ + F_2^+$	0.19	0.29	0.23	0.19	0.19
$CF_2^{2+} + F^+$	—	0.18	0.16	0.13	0.13
$F_2^+ + F^+$	—	0.12	0.09	0.09	0.08

Bonham (1993); however note, the Bruce and Bonham (1993) results were increased by a factor 1.18 to take into account the new instrumental efficiency (0.304) measurement from Bruce and Bonham (1994). The values from our earlier work are given in parenthesis in table 1 (Bruce *et al* 1992); these cross sections have also been corrected to account for the results from Bruce and Bonham (1993) and the new efficiency measurement (Bruce and Bonham 1994). The nominally lower values from Bruce *et al* (1992) are primarily accounted for by having used a much lower extraction field in that work (80 V cm^{-1} compared with 150 V cm^{-1} in the current work); this readily explains the largest discrepancy for the $C^+ + F^+$ ion pair—by far the hottest ion pair. Features observed for the first time are: $F^+ + F^+$, $CF_2^+ + F_2^+$, $CF^+ + F_2^+$, $CF_2^+ + F^+$ and $F_2^+ + F^+$; these cross sections are listed in table 1. Other new features observed but not listed in table 1 are: $C^+ + F_2^+$, $F^{2+} + F^+$ and $C^{2+} + F^+$ (e.g. see figure 2(*c*)); these features all had cross sections well under 10^{-21} m^2. The estimated uncertainties in the cross sections are 20% for the dominant channels (greater than 10^{-20} m^2) with the exception of the $F^+ + F^+$ channel; the uncertainty for that channel is 35% while the uncertainties in the lesser channels (cross sections under 10^{-20} m^2) are estimated to be 30%.

Due to interference with the 'diagonal' noise—described in Frasinski *et al* (1986)—the accuracy of the cross sections for $F^+ + F^+$ was much poorer. In order to determine these cross sections an estimate of the noise contribution cluttered very near the diagonal (t_A=t_B) was necessary. In general, the ratio of diagonal noise to the equivalent single ion intensity was relatively constant for a given ion pair over the range of electron impact energies used; however, since the ratio in percentage varied from 1–2% depending on the ion, it was necessary to determine the diagonal to single ion ratio specifically for the $F^+ + F^+$ pair. This correction was accomplished by measuring the ratio well below the threshold (35–40 eV) for true ion pair production.

Moreover, serious loss of signal occurs near the diagonal due to a 20 ns dead time for the constant fraction discriminator (CFD), hence coincidences within 20 ns were not counted in the experiment. This contribution was estimated and subsequently added to the data by determining the number of 'dead' channels, and estimating the counts that would have been in those channels by averaging the counts in the 'flat' zone of the $F^+ + F^+$ distribution (the 'flat' zone is the area of the distribution, usually emanating from the centre, that is relatively constant—a typical profile for a distribution with a fixed or narrow momentum distribution (Eland 1987)).

Table 2. Kurtoses ($\gamma_{t_{A,B}}$) computed for the dominant features (figures 3(*a*)–(*d*)) along the time axes t_A and t_B, respectively. The values have been averaged over the five electron impact energies used in the experiment, the numbers in parenthesis denote the deviation of the mean from the highest to lowest value. Also, the angles ϕ that the distributions make with the horizontal axis, t_A, are listed along with their standard errors. See discussion is section 4.2 for further details.

Ion pair	γ_{t_A}	γ_{t_B}	ϕ (deg)
$F^+ + CF_3^+$	−0.94 (+0.05, −0.06)	−0.60 (+0.12, −0.09)	47 ± 2
$F^+ + CF_2^+$	−0.81 (+0.04, −0.04)	−0.45 (+0.09, −0.05)	47 ± 2
$F^+ + CF^+$	−0.71 (+0.07, −0.09)	−0.35 (+0.07, −0.13)	46 ± 1
$C^+ + F^+$	+0.08 (+0.25, −0.16)	−0.68 (+0.12, −0.13)	67 ± 3

4.2. Interpretations of profiles

All three of the dominant features ($CF_3^+ + F^+$, $CF_2^+ + F^+$, $CF^+ + F^+$) had ϕ angles at or near 45° (determined by the method described in section 3) as measured clockwise from the horizontal (t_A) axis, indicative of the two ions detected carrying away the bulk of the momentum (i.e. principally two body break-up) in a Coulombic explosion. The major exception was $C^+ + F^+$, the angle increased monotonically from 63° at 100 eV to 69° at 500 eV. This suggests a rapid sequential reaction with initial charge separation:

$$CF_4^{2+} \rightarrow CF^+ + F^+ + (2F \text{ or } F_2) \tag{20a}$$

$$\downarrow$$

$$C^+ + F \tag{20b}$$

where step (20*a*) is much faster than molecular rotational times (sub-picosecond), while step (20*b*) is much slower than the molecular rotational time but much faster than the experimental time scale: 16 ns. In this reaction sequence, when the energy of the first step is large compared to the final step energy, the angle is approximately given by $\tan\phi = m(C + F)/m(C)$ (see Eland 1987) which is 69° in this case. This is in agreement with Codling *et al* (1991) who observed an angle of 69° with respect to t_A (fast ion) axis in photoionization studies (note that Codling measures his angles with respect to the slow ion axis, t_B); they also observed 45° for the other three reactions.

This picture is further supported by a statistical interpretation for bivariate data with random variables t_A and t_B (Eland 1987). By measuring the kurotsis of each profile temporally, using the counts as a weighting factor, one can determine how non-normal a distribution is. For instance, a square distribution has a kurtosis of −1.2 which would result from a single valued momentum, while a normal distribution is zero which would be the case for randomly distributed momenta. In table 2 the kurtoses computed from the measured data are summarized, the values listed are averaged over all five electron impact energies as they were all very similar for a given ion pair regardless of energy, the deviation of the mean from the highest and lowest value are also listed (an error bar is probably meaningless since we are dealing with second- and fourth-order moments—i.e., not normally distributed).

Most of the measured time distributions had kurtoses between −0.5 to −1.0, compatible with a temporal distribution with a relatively flat top and a slight tail in the wings, and commensurate with the momentum distributions shown in figures 5(*a*)–(*b*). Kurtoses associated with fluorine ions tend to be around −0.9 (more square temporal distribution with subsequent more narrowly peaked momentum) while those associated with carbon

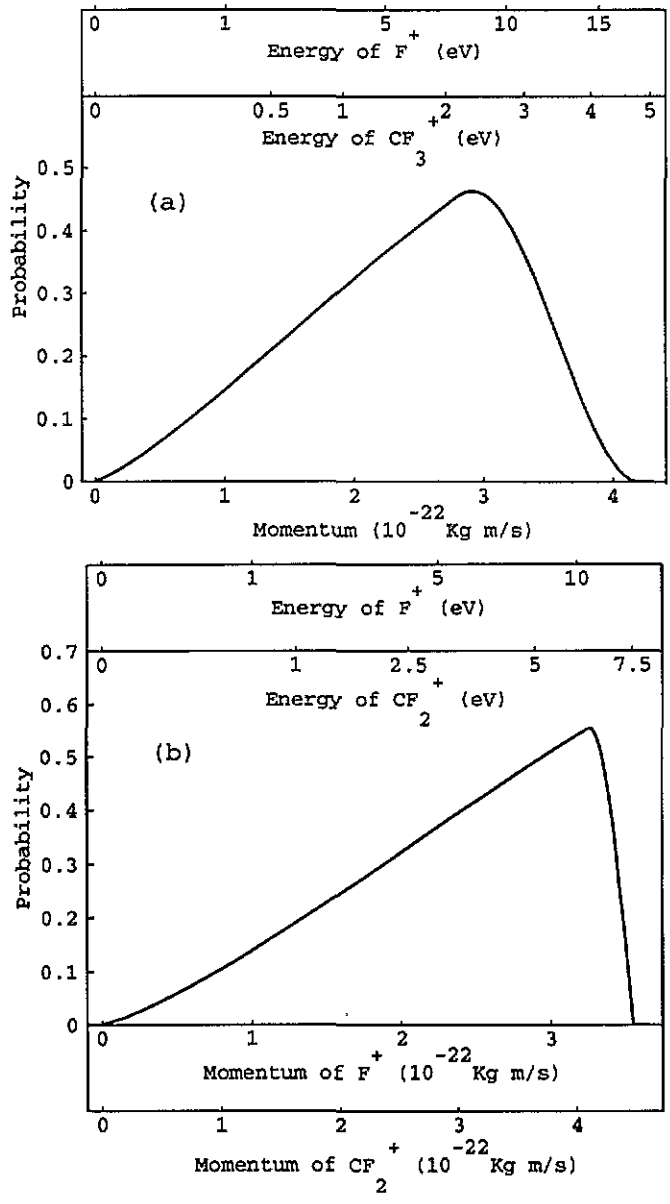

Figure 5. Momentum/energy distrubution plots for the dominant ion–ion coincidence features observed at an electron impact energy of 100 eV (see figures 3(*a*)–(*d*)): (*a*) $CF_3^+ + F^+$; (*b*) $CF_2^+ + F^+$; (*c*) $CF^+ + F^+$; (*d*) $C^+ + F^+$.

containing molecular ions tend to be lower, typically −0.5—intermediate between a normal and a square distribution—with the heavier molecular ions tending to be somewhat more negative and the lighter ions somewhat less negative (randomness of momentum distribution may be affected by rearrangement reactions during initial dissociation or sharing energy with rovibrational degrees of freedom). The major exception to this case is the temporal distribution associated with $C^+ + F^+$, the kurtosis for F^+ (t_A) averages −0.68 while the kurtosis for C^+ (t_B) averages +0.08 (the only positive value measured for any distribution);

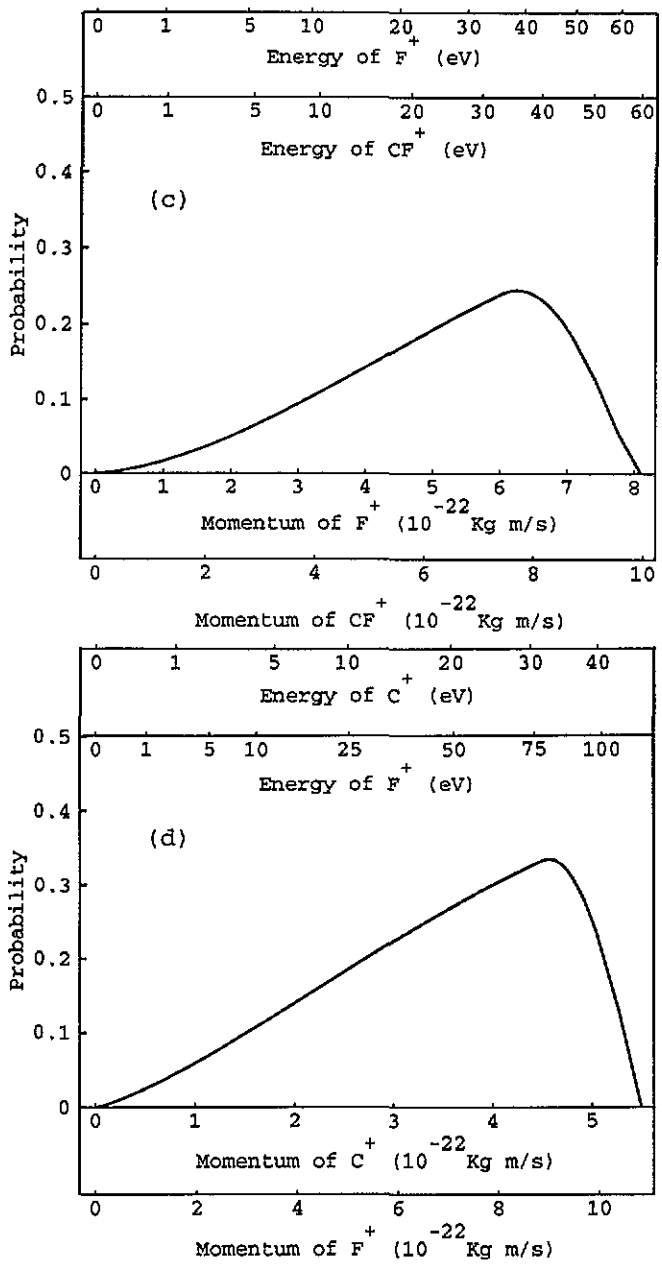

Figure 5. (Continued)

this indicates F^+ has a 'typical' distribution, as described above, for these reactions, but C^+ is almost perfectly normally distributed. This result could be produced by the reaction sequence listed in equations (20*a*, *b*); in the initial charge separation, F^+ will preserve its momentum distribution, while the subsequent dissociation, along with initial rearrangement reactions or rovibrational energy transfer in the molecular ion, will 'randomize' the C^+ momentum resulting in a normal distribution.

Table 3. Angles for molecular fragmentation of CF_4^{2+} obtained from Monte Carlo simulation. θ_{AB} is the angle between P_A and P_B, while θ_{BC} is the angle between P_B and P_C. The momentum scales for the neutral fragments in figures 5(*a*)–(*d*) can be determined by multipling $C_{AC} = P_C/P_A$ by P_A.

Ion fragments	θ_{AB} (deg)	θ_{BC} (deg)	C_{AC}
$F^+ + CF_3^+$	180	—	—
$F^+ + CF_2^+ + F$	133	128	0.93
$F^+ + CF^+ + (2F \text{ or } F_2)$	122	129	1.10
$C^+ + F^+ + (3F \text{ or } F+F_2)$	135	151	1.45

4.3. Results of Monte Carlo simulation

Momentum and energy distributions for the fragments of CF_4 based on the theory in section 3 are shown in figure 5; as well, the angles (θ_{AB}) between the ions and the angle (θ_{BC}) between the slowest ion (P_B) and the unobserved neutral momenta (P_C) are listed in table 3. The magnitude of the momenta vectors were determined for the fragment ions (labelled as P_A and P_B) along with the magnitude of the sum of the momenta vectors for the unobserved neutral fragments, the neutral fragment's momentum scale in figure 5 is obtained by multiplying the P_A scale by the constant $C_{AC} = P_C/P_A$ listed in table 3.

In figures 3(*a*)–(*d*), the dotted contours indicate the data from the Monte Carlo simulation while the full contour lines represent the actual data. As can be seen, the model agrees well with the $F^+ + CF_3^+$ data (simple two-body break-up) in figure 3(*a*) and relatively well for $F^+ + CF_2^+$ in figure 3(*b*); however, the fits are very poor for the other cases ($F^+ + CF^+$ and $F^+ + C^+$) with the agreement generally getting worse with higher degree of fragmentation. For the latter two reactions (figures 3(*c*) and (*d*)), the Monte Carlo contours could not be extended to agree with the data even when the kinetic energy of the reaction was allowed to exceed the limit imposed by conservation of energy; this is primarily due to greater ion losses in the TOF spectrometer as the ion velocity increases (conditions imposed by equation (18)). This indicates a severe breakdown of the simple model. The primary culprit is indicated by the statistical model discussed in section 4.2 which argues that sequential or multistep processes dominate. In these cases fragmentation times must be short compared to experimental time resolution (16 ns) but slow compared to molecular rovibrational times (i.e., greater than femtoseconds).

4.4. Tail on $CF_3^+ + CF_3^+$ distribution (evidence for unstable CF_4^+?)

The occurrence of tails on some of the mass peaks has also been observed. The most pronounced example of this emanates from the CF_3^+–CF_3^+ accidental coincidence peak, it shows a small but reproducible long time (high mass) vertical tail which existed at all electron impact energies (100 to 500 eV) and was not substantially reduced after covariant correction (i.e., see figures 2(*a*) and (*b*)). This means that a normal (prompt) CF_3^+ ion is detected in coincidence with a slower or more massive fragment. In this case it could either be CF_3^+ produced by a long lived reaction

$$CF_4^+ \rightarrow CF_3^+ + F \text{ or } F^* \tag{21}$$

a metastable neutral, or both (a metastable or excited state might have sufficient internal energy to trigger the detector). If a very long lived metastable neutral ($\tau \gg 10\ \mu s$) was involved, it would have a very unique signature. The tail should show little if any intensity fall off with increasing flight time since such neutrals would be continuously arriving during

the experiment due to their long flight times; absence of an equally strong horizontal tail suggest the species responsible for the vertical tail must be coming from the same experiment since species present from previous experiments would be counted principally as single events (time-to-digital converter (TDC) is cleared prior to each experiment). An ion of mass M, on the other hand, should behave very differently. The time required for an ion with no initial kinetic energy to traverse the draw out region will be

$$\Delta t_1 = L_1 \left(\frac{2M}{E_1}\right)^{1/2} \tag{22}$$

where $L_1 = 6$ mm and E_1 is 90 eV. The time required to traverse the first constant field region will be

$$\Delta t_2 = \frac{L_2}{2} \left(\frac{2M}{E_1}\right)^{1/2} \tag{23}$$

where L_2 is 25 mm. The time for traversal of the second acceleration section of length $L_1 = 6$ mm is given as

$$\Delta t_3 = L_1 \left(\frac{2M}{E_2}\right)^{1/2} \left[\left(1 + \frac{E_1}{E_2}\right)^{1/2} - \left(\frac{E_1}{E_2}\right)^{1/2}\right] \tag{24}$$

where E_2 is the additional kinetic energy imparted to the ion, $E_2 = 510$ eV. The final constant field drift section requires a transit time of

$$\Delta t_4 = \frac{L_3}{2} \left(\frac{2M}{E_2}\right)^{1/2} \left(1 + \frac{E_1}{E_2}\right)^{-1/2} \tag{25}$$

where the flight distance L_3 is 150 mm. The transit time for the final acceleration region is

$$\Delta t_5 = L_1 \left(\frac{2M}{E_3}\right)^{1/2} \left[\left(1 + \frac{E_1 + E_2}{E_3}\right)^{1/2} - \left(\frac{E_1 + E_2}{E_3}\right)^{1/2}\right] \tag{26}$$

where the additional kinetic energy imparted to the ion is 2750 eV. The total flight time of the ion will be the sum of equations (22)–(26); however, note an experimentally determined offset constant (t_0) must be added to take into account delays in the electronics and therefore make the TOF agree with figures 2(*a*)–(*c*). If the L_n, $n = 1$–5, are expressed in cm, the kinetic energies in eV and the ion mass in atomic mass units then equations (22)–(26) must be multiplied by the conversion factor 1.02 μs cm^{-1} eV$^{1/2}$ amu$^{-1/2}$. These simplified equations predict a total flight time of 7.03 μs for the CF_4^+ ion for our apparatus and a flight time of 6.22 μs for the CF_3^+ ion. Any CF_4^+ ion which makes it into the field-free region 4 (Δt_4) before decomposing into CF_3^+ will arrive at the detector within 12 ns of the flight time expected for CF_4^+ itself (assuming little or no internal energy released) since the velocity, and hence the TOF, remains constant in the drift region 4 regardless of the mass (e.g., see Landau and Lifshitz 1976 p 41), the small difference being due to acceleration in region 5. If the lifetime for the break-up is of the order of several μs then we would expect to observe a peak at the mass for CF_4^+ . In fact, since the flight time for CF_4^+ out to the beginning of region 4 is 2.87 μs, the ratio of the area of the mass peak at the expected flight time for CF_4^+ to the total area observed for the tail will be 0.06 if the lifetime is 1 μs.

Failure to observe a ratio above the 6% level would be clear evidence that the lifetime was less than 1 μs. A lifetime of about 4 μs would have $\sim$ 50% of the decay tail area in the CF_4^+ peak. Hence we can expect the experiment to be sensitive to lifetime effects providing that the lifetimes are longer than the time resolution of the experiment.

In terms of the experimental results shown in figures 2(*a*)–(*c*), the exponential decay between the expected positions for the CF_3^+ and CF_4^+ mass peaks argues for the existence of a metastable state of CF_4^+ with a lifetime less than 1 μs (Deutsch *et al* (1985) and Schmidt and Seefeldt (1989) have observed metastable CF_4^+; the first authors put the lifetime in the 3-10 μs range while the later claim a lifetime of 15 μs). The remaining long tail at flight times longer than that expected for CF_4^+ would have to be caused by metastable neutral species or, possibly, neutrals produced by dissociation of an ion occuring after the ion has achieved a kinetic energy in one of the acceleration regions sufficient for the neutral to produce a signal in the detector. Hence, the primary channel is believed to be reaction (21) with metastable F* which has been observed in abundance by van der Burgt and McConkey (1991).

There is further evidence for CF_4^+ in the single ion spectra, an extremely weak peak is sometimes observed in unusually long experiments where CF_4^+ is expected; the lifetime and cross section are related by

$$\sigma_{\text{eff}}(t) = \sigma_{CF_4^+} e^{-t/\tau} \tag{27}$$

where τ is the lifetime of reaction (21), $t = \sum_{n=1}^{3} \Delta t_n$ is the flight time to region 4 (2.87 μs), and $\sigma_{\text{eff}}(t)$ is the effective cross section for flight time t. The estimate for $\sigma_{\text{eff}}(t)$ from the data in figures 2(*a*) and (*b*) is $\sim 10^{-4}$ Å^2. The main difficulty in determining the cross section (and lifetime) is that CF_4^+ is embedded on top of a broad tail emanating from CF_3^+ in the single event spectra (very similar to the coincident spectra) well past where CF_4^+ is expected (believed to be due to metastable F); this contribution was subtracted out when estimating $\sigma_{\text{eff}}(t)$. If the lifetime is very long ($\tau \gg 10$ μs) $\sigma_{CF_4^+} \cong \sigma_{\text{eff}}(t)$, while if $\tau = 1$ μs the cross section is $\sim 10^{-3}$ Å^2, and correspondingly higher for shorter lifetimes.

Finally, in addition to unimolecular decay from reaction (21), one additional complication can arise in the measurement which decomposes CF_4^+; namely, collision induced reactions (Deutsch *et al* 1985)

$$CF_4^+ * + CF_4 \rightarrow CF_3^+ + CF_4 + F \text{ or } F^* \tag{28}$$

can dissociate the ion while it is being transported down the flight tube; however, we estimate this effect to be small at the background pressures used in the experiment ($\sim 10^{-6}$ Torr) based on the reaction rates measured in Deutsch *et al* (1985) and Schmidt and Seefeldt (1989) for process (28).

It should be noted that lifetime information is not limited to accidental coincidence peaks. In fact, the observation of a tail on a non-accidental coincidence peak associated with a three or more body break-up reaction would be a clear signal for a two step reaction in which the first step involved a fast two ion break-up followed by a slow break-up of one of the two ions into an ion and one or more neutral fragments. If the break-up in to two ions is the slow step then the coincidence peak will be elongated along its major axis.

4.5. Appearance potentials

Appearance potentials for the dominant features have been determined in previous works (Bruce *et al* 1992, Codling *et al* 1991). In this work, due to the amount of time it takes to collect data as described in section 2, no effort was made to accurately determine the appearance potentials.

5. Conclusions

Covariance mass spectrometry has proven to be an invaluable tool for the study of molecular fragmentation whatever the excitation source (e.g., photons (Eland 1987, Codling *et al* 1989, 1990, 1991) or electrons (this work)) providing such information as fragmentation momenta and energy. It is particularly invaluable in ascertaining cross sections that may be ambiguous in a conventional study. In many of these previous studies each ion recorded was counted as a single isolated event, with no accounting for true coincident events, which led to misinterpretations of cross section data (namely, the counting cross section). Hence, with cross-correlation or covariance mapping mass spectrometry, more accurate mass abundances can be obtained; furthermore, it offers an enhanced capability of differentiating between ambiguous mass ions in gas mixtures (e.g. N_2O or CO_2 in an air). It is also obvious from this work that the technique can be expanded to study neutral metastable coincidences (i.e., see section 4.4) providing that the internal energies of the metastables are sufficient to trigger the ion detector. The ideal system would use a reflectron TOF for detecting ions in coincidence with a line-of-sight detector for neutral metastables (e.g., see Hagan *et al* (1993)).

The instantaneous explosion model was shown to yield good agreement for the two and three body break-up reaction but failed badly in the cases of four and more body break-ups. We also attempted to fit several multi step mechanisms to these latter cases but found them to yield ambiguous results because of the over flexibility of the model created by the additional parameters involved. Usually the multi step models involve a slow step. When the time resolution of the experiment becomes less than the lifetime of the slowest step it should be possible to establish the mechanism for the reaction. Hence, we feel that further progress in this direction will have to wait for improvements in the experiment. As of now, the most useful method for interpreting data on three and more body break-up reactions appears to be the statistical method discussed in section 4.2.

Finally, since CF_4 is readily used as an etchant gas in plasma processing, a few words are in order about the implications of this study to that endeavor. Even at high ion sheath potentials, CF_4 has been a difficult gas to make anisotropically etch Si under reactive ion etching (RIE) conditions. H_2 can be added to make CF_4 anisotropically etch by scavenging the fluorine and thereby enhancing polymer formation, but this scheme favors SiO_2 etching at the expense of Si; on the other hand, O_2 can be added to make it more selective over SiO_2 by scavenging CF_x radicals (primary polymer precursors) but the anisotropy is extremely poor (e.g., see Flamm *et al* 1984). Based upon the current and previous works in this lab, we believe there are two culprits at work, one involving neutral fluorine and the other highly energetic ions produced by electron collisions. Firstly, in the previous studies, neutral fluorine has been shown to be the most abundant radical produced by electron collisions and has been observed to have mean kinetic energies around 8 eV (Bruce *et al* 1992, Ma *et al* 1991); with radicals so abundant and hot, it is not surprising that a deleterious effect is observed when etching with this radical (Summerer and Kushner 1991). Furthermore, in the current work, it has been shown that at electron impact energies above 40 eV (typical of ion sheath potentials in RIE) double ions produce extremely energetic neutrals and ions in violent Coulombic explosions with kinetic energies well in excess of 8 eV (see figures 5(*a*)–(*d*)). Note that in the reaction shown in figure 5(*b*) neutral fluorine atoms are produced with kinetic energies which are 86% (see the value for C_{AC} in table 3) of the values for F^+. Furhermore, it should be noted from table 1 that these reactions can account for as much as 15% of the gross ion production and 50% of the F^+ production. In the case where O_2 is added, one is left with almost exclusively hot F and F^+. These high kinetic energies can

be imparted to the lateral dimension while the ions are being accelerated across the sheath thereby attacking the side walls and making the achievement of anisotropy difficult.

Acknowledgments

The authors wish to acknowledge support of this work under NSF grant PHY 9214126.

References

Becker R A 1954 *Introduction to Theoretical Mechanics* (New York: McGraw-Hill)
Besnard-Ramage M J, Morin P, Lebrun T, Nenner I, Hubin-Franskin M J, Lablanquie P and Eland J H D 1989 *Rev. Sci. Instrum.* **60** 2182
Brink D M and Satchler G R 1968 *Angular Momentum* (Oxford: Clarendon)
Bruce M R and Bonham R A 1992 *Z. Phys.* D **24** 149
—— 1993 *Int. J. Mass Spectrom. Ion Proc.* **123** 97
—— 1994 *J. Mol. Structr.* to be published
Bruce M R, Ma C and Bonham R A 1992 *Chem. Phys. Lett.* **190** 285
Codling K, Frasinski L J and Hatherly P A 1989 *J. Phys. B: At. Mol. Opt. Phys.* **22** L321
Codling K, Frasinski L J, Hatherly P A and Stankiewicz M 1990 *Phys. Scr.* **41** 433
Codling K, Frasinski L J, Hatherly P A, Stankiewicz M and Larkins F P 1991 *J. Phys. B: At. Mol. Opt. Phys.* **24** 951
Creasey J C, Lambert I R, Tuckett R P, Codling K, Frasinski L J, Hatherly P A, Stankiewicz M and Holland D M P 1990 *J. Chem. Phys.* **93** 3295
Curtis D M and Eland J H D 1985 *Int. J. Mass Spectrom. Ion Proc.* **63** 241
Deutsch H, Leiter K, and Mark T D 1985 *Int. J. Mass Spectrom. Ion Proc.* **67** 191
Eland J H D 1987 *Mol. Phys.* **61** 725
Eland J H D and Mathur D 1991 *Rapid Commun. Mass Spectrosc.* **5** 475
Eland J H D, Wort F S, Lablanquie P and Nenner I 1986a *Z. Phys.* D **4** 31
Eland J H D, Wort F S and Royds R N 1986b *J. Electron Spectrosc. Relat. Phenom.* **41** 297
Flamm D L, Donnelly V M and Ibbotson D E 1984 *VLSI Electronics Microstructure Science: Plasma Processing for VLSI* vol 8 ed N G Einspruch and D M Brown (Orlando, FL: Academic) p 190
Frasinski L J, Codling K and Hatherly P A 1989a *Phys. Lett.* **142A** 499
—— 1989b *Science* **246** 1029
Frasinski L J, Hatherly P A and Codling K 1991 *Phys. Lett.* **156A** 227
Frasinski L J, Stankiewicz M, Randall K J, Hatherly P A and Codling K 1986 *J. Phys. B: At. Mol. Phys.* **19** L819
Hagan D A and Eland J H D 1991 *Rapid Commun. Mass Spectrosc.* **5** 512
Hagan D A, Eland J H D, and Lablanquie P 1993 *Int. J. Mass Spectrom. Ion Proc.* **127** 67
Hatherly P A, Frasinski L J, Codling K, Langley A J and Shaikh W 1990 *J. Phys. B: At. Mol. Opt. Phys.* **23** L291
Hatherly P A, Stankiewicz M, Frasinski L J, Codling K and MacDonald M A 1989 *Chem. Phys. Lett.* **159** 355
Landau L D and Lifshitz E M 1976 *Mechanics* 3rd edn (Oxford: Pergamon)
Ma C, Bruce M R and Bonham R A 1991 *Phys. Rev.* A **44** 2921
—— 1992 *Phys. Rev.* A **45** 6932
McCulloh K E, Sharp T E and Rosenstock H M 1965 *J. Chem. Phys.* **42** 3501
Schmidt M and Seefeldt R 1989 *Int. J. Mass Spectrom. Ion Proc.* **93** 141
Stankiewicz M, Hatherly P A, Frasinski L J, Codling K, and Holland D M P 1989 *J. Phys. B: At. Mol. Opt. Phys.* **22** 21
Summerer T J and Kushner M J 1991 *J. Appl. Phys.* **70** 1240
Ueda K, Shigemasa E, Sato Y, Yagashita A, Sasaki T and Hayashi T 1989 *Rev. Sci. Instrum.* **60** 2193
Van der Burgt P J M and McConkey J W 1991 *J. Phys. B: At. Mol. Opt. Phys.* **24** 4821
Winkoun D and Dujardin G 1986 *Z. Phys.* D **4** 57